



Functionalization of bacterial nanocellulose-based wound dressing for increased drug retention

Troy C. Breijaert^a, Marina Fontes^b, Paula de Abreu Fernandes^c, Hernane da Silva Barud^{c,d}, Sidney J.L. Ribeiro^d, Gulaim A. Seisenbaeva^{a,*}

^a Department of Molecular Science, Swedish University of Agricultural Science, Uppsala, 756 51 Ultuna, Sweden

^b Department of Chemistry, Federal University of São Carlos (UFSCar), São Carlos, 13565-905, SP, Brazil

^c Department of Biotechnology, University of Araraquara (UNIARA), 14801340, Araraquara, SP, Brazil

^d Institute of Chemistry, São Paulo State University – UNESP, Araraquara, SP, 14800-900 Brazil

ARTICLE INFO

Keywords:

Bacterial nanocellulose
Wound dressing
Phosphorylation
Drug delivery
Titania

ABSTRACT

Bacterial nanocellulose is a fascinating biopolymer with immense application potential, including as a wound dressing material. It is highly biocompatible and capable of keeping humidity needed for wound healing. However, it lacks specific affinity to pharmaceuticals to be delivered in a controlled fashion in a topical application, urged by the necessity to decrease the release of medicines to the environment. Solving this problem requires tailoring of the material functionality by chemical modification. In this work, a two-step strategy applying first phosphorylation and then introduction of biocompatible mineral particles was applied. Surface modification of commercially available wound dressing material based on dried bacterial nanocellulose led to phosphate grafting of 1.5–1.8 mmol/g and then uniform coverage of individual fibers (colloidal TiO₂) or formation of aggregated platelets (TiBALDH®) on the surface (with Ti:P element ratios 0.45–0.80). To the titania functionalized dressing the broad spectrum antibiotic Tetracycline was bound (41–45 mg g⁻¹) with its release delayed over several hours / days (over 50 % in 120 h for both nanocarriers). Biological essays indicated excellent biocompatibility and improved cell adhesion, offering a path to accelerated wound closure, promising for diverse tissue engineering applications. This study demonstrated a strategy in approach to dressing materials with delayed drug release properties exploiting the affinity of pharmaceuticals to mineral nanoparticles.

1. Introduction

Materials for wound treatment are highly requested and attract continuous attention of researchers. A paramount aim in wound management is preventing bacterial infection. Commonly used wound dressing materials function by providing a physical barrier against infection caused by microorganisms, passively protecting against infection (Stoica, Chircov & Grumezescu, 2020). Therefore, antibiotics are often prescribed per-orally for systemic treatment. This results in consuming large quantities of antibiotics and their distribution into wastewater streams through excretion, leading to water streams becoming increasingly polluted by residual pharmaceuticals (Malnes et al., 2022). Exposed to increasing background concentrations of antibiotics, bacteria are becoming increasingly resistant against them, which has led to augmented interest in alternatives such as local, topical application of antibiotics for wound management.

The emergence of nanotechnology has opened up avenues for the production of active wound-dressing materials, which facilitate wound healing, exert antibacterial properties and/or stimulate tissue regrowth (Moritz et al., 2014; Li et al., 2020). Inorganic nanoparticles for example, have been reported to improve wound healing (Seisenbaeva et al., 2017; Paladini & Pollini, 2019) and they have been proven to facilitate controlled release of antibiotics (Galkina et al., 2015a; 2015b). Combining the attractive properties of inorganic nanoparticles with natural polymers, allows for the creation of hybrid materials with unique properties, which can be used for drug delivery.

Bio-based polymers such as cellulose have increasingly been addressed as matrices for active inorganic components. Cellulose is the most abundant natural polymer on the planet, accounting for 1.5 × 10¹² tons of annual biomass production (Klemm, Heublein, Fink & Bohn, 2005). It is a linear homopolymer comprised of β-1,4-linked glycopyranose (O'Sullivan, 1997; Marchessault & Sundararajan, 1983). It is

* Corresponding author.

E-mail addresses: hsbarud@uniara.edu.br (H.S. Barud), gulaim.seisenbaeva@slu.se (G.A. Seisenbaeva).

<https://doi.org/10.1016/j.carpta.2025.100756>

found in the cell wall of plants, in seaweed, and in fungi. In addition, it is produced by some species of bacteria, such as *Komagataibacter Xylinus* (formerly *Acetobacter* and *Gluconacetobacter*) which forms a biofilm comprised of cellulose (Brown, 1886). Cellulose and its derivatives have a long history in the pharmaceutical industry in various types of formulations as it is biodegradable, non-toxic, non-carcinogenic and biocompatible (Thoorens et al., 2014). Nanocellulose for biomedical applications can be produced from many different sources such as wood, cotton or even fruit peel waste (Datta et al., 2024).

Bacterial nanocellulose (BNC) is a type of cellulose with major advantages over vegetal (plant) cellulose, owing to its unique native purity (Klemm, Schumann, Udhardt & Marsch, 2001). It is produced by fermentation and only contains microbial cells, nutrients and secondary metabolites, which can easily be removed to produce highly pure cellulose. By comparison, vegetal cellulose contains by-products such as lignin, pectin and hemicellulose (Klemm, Heublein, Fink & Bohn, 2005). BNC has outstanding physical and mechanical properties, which emerge from its unique 3D structure. BNC aggregates to form long aggregated microfibrils with a width of 70–150 nm in a reticular network which provides the material with high surface area, elasticity and flexibility (Klemm, Heublein, Fink & Bohn, 2005; Fink, Purz, Bohn & Kunze, 1997). BNC has many intrinsic characteristics that make it an ideal wound dressing material, especially for burn wounds, temporary skin substitutes or tissue regeneration as it has the capacity to absorb exudates from injured tissue and accelerate granulation (Khalid et al., 2017; Li et al., 2015). A major drawback in using BNC and other celluloses for wound dressing applications however, is a lack of antibacterial activity intrinsic to the material, meaning that wounds can easily become infected if not properly managed.

In order to overcome this challenge, antibacterial agents such as silver nanoparticles have been added to cellulose materials in order to grant it antibacterial properties (Barud et al., 2011; Volova et al., 2018). Silver nanoparticles though have been shown to be cytotoxic due to the generation of ROS by the particles itself or through the release of silver ions (Liao, Li & Tjong, 2019; Tripathi & Goshisht, 2022). An alternative approach is loading cellulose materials with antibiotics. However, cellulose itself has a low retention for many drugs and there is a risk that rapid release of drugs may have toxic effects (Horue et al., 2023).

BNC benefits from having a highly porous structure in its native state, which has been used to imbue the material with antibacterial properties by loading metal/metal-oxide nanoparticles with antibacterial properties (Khalid et al., 2017; Volova et al., 2018; Li et al., 2017) or loading pharmaceuticals for delayed drug release (Moritz et al., 2014). Nanosized TiO₂ in particular has been garnering attention as it is considered biocompatible with low toxicity. It has been demonstrated that depending on the surface chemistry involved, titania induces blood coagulation (Seisenbaeva et al., 2017; Svensson et al., 2021; Ekstrand-Hammarström et al., 2015), which promotes wound-healing by initiating an immune response (Seisenbaeva et al., 2017). Titania derived from ammonium oxo-lactato titanate by comparison has been shown to cause minimal coagulation activation, which makes it suitable for applications where coagulation is undersired (Svensson et al., 2021). Frequently reported methodology for imbuing BNC with antibacterial properties often relies on impregnating the material with nanoparticles and/or pharmaceuticals within the porous substrate, without the formation of a chemical bond, followed by lyophilizing or supercritical drying of the material, potentially leading to the release of nanoparticles into the wound environment with all consequences that entails.

Another specific limitation of using BNC is its limited swelling capacity post-drying (Klemm, Heublein, Fink & Bohn, 2005), requiring the material to be impregnated before drying. Thus, this strategy would find limited use for materials like dry BNC sheets that currently are available as wound dressing material. In the past several articles have reported the use of chemically bonded metal oxide-cellulose hybrid materials for controlled drug delivery (Galkina et al., 2015a; Galkina et al., 2015b; Gaio et al., 2022; Breijaert et al., 2022). To the best of our knowledge,

nanocomposites of dry BNC wound dressing with chemically grafted metal oxides onto the surface for enhanced uptake and controlled release of pharmaceuticals have not been reported. The aim of the current work was to produce a bacterial nanocellulose based material loaded with antibiotics for controlled release. Improved retention of antibiotic drug was achieved through surface grafting of inorganic functional components such as nano titania. Two types of very uniform TiO₂ nanoparticles about 3.5 nm developed in our previous studies – the triethanol ammonium terminated titania (TATT) (Seisenbaeva et al., 2017; Kessler, Seisenbaeva, Håkansson & Unell, 2008), easily desorbing the capping ligands and highly active in blood coagulation, and the particles generated by an equilibrium described for “Dihydroxybis(ammonium lactato)titanium(IV)” (TiBALDH®), which are strongly surface capped by lactate ligands and not producing blood coagulation effects (Seisenbaeva et al., 2017; Seisenbaeva, Daniel, Nedelec & Kessler, 2013). Insights were gained into how this material would behave in tissue regeneration applications testing biocompatibility, cell adhesion and pseudo wound closure effects.

2. Materials and methods

2.1. Materials

“Dihydroxybis(ammonium lactato)titanium(IV)” (TiBALDH®) 50wt % aqueous solutions (~2.08 M Ti) were obtained from Fischer Scientific. It contains highly crystalline anatase nanoparticles terminated by lactate ligand, 3.5 nm in diameter. Triethanol ammonium terminated titania (TATT) was obtained according to literature, i.e., titanium ethoxide was first modified with triethanolamine and then the product was hydrolysed by diluted nitric acid solution in water-ethanol medium (Kessler, Seisenbaeva, Håkansson & Unell, 2008). The product has been characterized by multitude of techniques as anatase nanoparticles with an amorphous shell, 3.5 nm in diameter. Ammonium hydrogenphosphate was obtained from Kebo Lab AB, Urea was obtained from Sigma-Aldrich. Dry Bacterial nanocellulose sheets were obtained from BioSmart Nanotechnology LTDA, Araraquara, Brazil. Phalloidin-iFluor 488 (ab176753) was obtained from Abcam Ltda. Rabbit Recombinant Monoclonal anti-Collagen I conjugated to Alexa Fluor® 594 and Rabbit Recombinant Monoclonal anti-Fibronectin conjugated to Alexa Fluor® 555 also were obtained from Abcam Ltda. All chemicals were used without further purification. Water was purified using a Millipore system.

2.2. Synthesis

2.2.1. Bacterial nanocellulose

Bacteria cultures were manipulated inside a laminar flow hood, using sterilized lab ware. Bacterial nanocellulose sheets were grown by culturing *Komagataibacter Rhaeticus* (AF-1) (Machado et al., 2016) bacteria onto Hestrin-Schramm agar, containing D-glucose, yeast extract, peptone, disodium hydrogen phosphate, citric acid, agar and deionized water. The resulting inoculated HS agar plates were incubated in an air circulating oven for 72 h at 28 °C. The *K. rhaeticus* colonies were transferred to liquid Hestrin-Schramm medium and incubated for a further 72 h at 28 °C. After this period, a BNC pellicle had formed at the air-liquid interface, indicating the culture medium showed the appropriate conditions to produce a large bacterial nanocellulose sheet. The liquid culture media was transferred to trays together with fresh HS liquid media and cultured for 96 h at 28 °C. The produced hydrated bacterial nanocellulose pellicles were washed with distilled water to get rid of excess growth media, placed in 0.1 % aqueous NaOH and heated to 70 °C to remove bacteria. The wet BNC membranes were compressed and dried.

2.2.2. Phosphorylated bacterial nanocellulose

The general procedure by Ait Benhamou et al. (Ait Benhamou et al.,

2021) was modified for use with large aspect ratio bacterial nanocellulose sheets. In order to phosphorylate bacterial nanocellulose sheets a solution of 450 mg (3.91 mmol) $\text{NH}_4\text{H}_2\text{PO}_4$, 1.2 g (19.98 mmol) urea, 10 ml ultrapure water was prepared. In a petridish was placed 10×10 cm of a dry bacterial nanocellulose sheet material and allowed to soak overnight at room temperature under continuous agitation. After soaking overnight, the sheet was transferred to a wide ceramic plate and placed in a 160 °C oven for variable amounts of time (0–60 min). For the preparation of a phosphorylated bacterial sheet used for functionalization with drug and nano titania, the soaked bacterial nanocellulose sheet was placed at 160 °C for 20 min.

2.2.2.1. TiO_2 functionalized phosphorylated bacterial nanocellulose. For functionalization of a bacterial nanocellulose sheet, an approximately 5×5 cm sheet of bacterial nanocellulose was suspended in 5 ml ultrapure water, followed by the addition of 10 mmol of TiBALDH 50wt% solution per gram of bacterial nanocellulose. The sheets were allowed to soak overnight under continuous agitation and thoroughly washed with ultrapure water prior to analysis. For the preparation of TATT-coated cellulose sheets the same molar ratio of TATT to phosphate was used, however the sheets were allowed to soak over several days.

2.3. Characterization

Samples were characterized using a Bruker Dimension FastScan Bio Atomic Force Microscope (AFM) with a Nanoscope V controller in ScanAsyst mode using a Fastscan-B AFM probe (Silicon tip, f_0 :400 kHz, k:4 N/m, Tip radius: 5 nm nominally) and a scan rate of 1–3 Hz. Data was processed using Gwyddion 2.56 with align rows-median to remove skipping lines.

Scanning Electron Microscopy (SEM) observations of bacterial nanocellulose were conducted using a Hitachi FlexSEM 1000 at an acceleration voltage of 3–7 kV, spot size 20, and 5 mm working distance. For Energy Dispersive X-ray Spectroscopy (EDS) an acceleration voltage of 15 kv, spot size 50 and 10 mm working distance were used.

The Thermogravimetric analyzes (TGA) were performed to determine the thermal degradation, mass loss, thermal stability, degradation temperature (Tonset) and maximum degradation temperature (Tmax) of membranes. TG curves were obtained in an equipment TGA-SDT Q600/TA Instruments. The samples were heated at 25 to 600 °C at $10^\circ\text{C min}^{-1}$ under a nitrogen atmosphere. The experimental parameters' adjustments were made in OriginPro 9.0 software.

Solid-state ^{13}C NMR spectra were recorded on a Bruker Avance III HD 300 spectrometer (Germany) operating at a magnetic field strength of 7.04 T and a Larmor frequency of 75.00 MHz. The analyses were conducted using a 4 mm MAS probe with ZrO_2 rotors (and Kel-F covers) at a spinning rate of 9000 Hz. A relaxation time of 1 s and a 90° pulse of 2.6 μs were applied, utilizing magic-angle spinning and cross-polarization techniques. The chemical shifts were indirectly standardized through a sample of glycine, with carbonyl sign at 176.00 ppm in relation to the TMS which is the primary standard.

The degree of polymerization (DP) of bacterial nanocellulose (BNC) was determined by viscometry using an Ostwald viscometer according to Brazilian technical standard NBR7730.

For Cell Adhesion Assays a JEOL JSM-IT500HR SEM was used, using a working distance of 8 mm and an acceleration voltage of 5 kV (Paschoalin et al., 2017). Samples were prepared on carbon tape without any special treatment.

Fourier Transform Infrared (FTIR) analysis was done on a Perkin Elmer Spectrum 100 FT-IR Spectrometer using an ATR module or a window.

Titration was performed using a Metrohm Titrand 888 (2.888.0310), fitted with a 856 conductivity module (2.856.0010), 800 Dosino (2.800.0010), 5-ring conductivity measuring cell ($c = 0.7$, 6.0915.100), using TIAMO Light 2.5 as automation software. Titres were

determined using tris(hydroxymethyl)aminomethane (HCl) and potassium hydrogen phthalate (NaOH). Phosphate content was determined via conductometric titration by titration of protonated phosphate.

Immunofluorescence images were acquired using the Zeiss LSM800 Confocal Fluorescence Microscope.

Powder X-ray Diffraction (PXRD) data was obtained on a Bruker D8 QUEST ECO diffractometer equipped with a Proton III Area Detector and graphite-monochromated $\text{Mo-K}\alpha$ ($\lambda = 0.71073 \text{ \AA}$) radiation source. Data was processed with the EVA-12 software package. As a Mo-source ($K\alpha = 0.7093 \text{ \AA}$) is used instead of the standard Cu-source ($K\alpha = 1.5406 \text{ \AA}$) there is a loss in angular resolution as short wavelengths contract the diffraction pattern towards low Bragg angles. In order to compare cellulose samples, idealized cellulose structures (French, 2014) were used to simulate a powder diffraction patterns for cellulose I α , I β and cellulose II. Powder diffraction patterns were simulated between 5 and 50 2θ using Mercury software with Molybdenum as a source ($K\alpha = 0.7093 \text{ \AA}$) and FWHM: 1.5 as this closely resembles the angular resolution of the x-ray machine available and can be found in the supporting information (Sup. Fig. S10). Scherrer equation is exploiting full width of an intense X-ray peak at its half height to determine the size of a diffracting domain. Crystallite sizes were calculated using the Scherrer equation.

2.4. Tetracycline adsorption and desorption

In order to prepare a tetracycline loaded TiO_2 -Bacterial nanocellulose composite, a sheet containing TiO_2 was placed in a 100 mL Duran bottle together with a 70 mg/L tetracycline solution and sealed. The drug was allowed to adsorb at 55 °C overnight, drug loading was calculated by measuring the concentration before and after adsorption. For desorption experiments the sheet was placed in a 100 mL Duran bottle, followed by the addition of 50 ml citrate buffer (0.02 M, pH 6) and continuously stirred for the entire duration. Periodically 1 mL aliquots were taken for UV-Vis measurement and returned. Desorption was measured over a period of 130 h / 5–6 days.

2.5. Indirect cytotoxicity assay

To assess the cytocompatibility of the functionalized BNC composites, cytotoxicity test was performed according to the International Organization for Standardization (ISO 10,993–5/10,993–12) norms, using the extract dilution method MTT assay. L929 murine fibroblasts cells and human osteoblast-like SaOS-2 cells were obtained from the American Type Culture Collection (ATCC, VA, USA). For detailed protocol see supplementary materials.

2.6. Evaluation of pseudo-wound closure

Fibroblast (L929) and osteoblasts (SaOS-2) cells were cultured at a density of 1×10^5 cells/well in a 24-well plate, respecting the same conditions of temperature and percentage of CO_2 . The extraction media (treatments) were prepared following the same procedure described in Section 2.5. Subsequently, the confluent monolayer was confirmed 24 hours later, and then the wells were washed twice with PBS and the scratching of the cell layer was performed using a 200 μL pipette tip. To achieve straight scratches a ruler was used as a guiding device, as elucidated in Supplementary materials Fig. S1.

The cell free gaps were imaged in an inverted optical microscope (Nikon®) with a 10x objective. To ensure that pictures were always taken at the same position, a black line on the lower outside of the wells was made using a pen. The micrographs were taken above the black line at 0, 6, 24 and 48 hours until full closure of pseudo-wounds. The size of the pseudo-wounds was measured at all time points using ImageJ2 (Rueden et al., 2017). All samples were performed in triplicate. The closure (%) of the pseudo-wounds was calculated according to Equation 1 (Morais et al., 2023; Cappiello, Casciaro & Mangoni, 2018):

$$\% \text{ pseudo-wound closure} = \frac{\text{Area } t(0) - \text{Area } t(x)}{\text{Area } t(0)} \times 100$$

Where (x) corresponds to the time each micrograph was recorded.

2.7. Cell adhesion assay

For the cell adhesion studies, the same cell lines (SaOS-2 and L929) previously described were used. First, cells (5×10^4 cells/well) were seeded on functionalized BNC films (1 cm^3) inserted into the 24-well plate and grown for 72 h at 37°C with 5 % CO_2 . At the end of incubation, the media was removed, and cells were washed with sterile filtered 0.01 M PBS at pH 7.4. Next, the cells were fixed with 3 % glutaraldehyde in 0.01 M PBS for 0.5 h at room temperature. After washing with 0.01 M PBS, samples were dehydrated through an ascending ethanol series (30 %, 50 %, 70 % and 95 %, 3 min each) with a final incubation in 100 % ethanol for 3 min (repeated 2 times). Dry samples were sputter coating to generate a 10-nm carbon layer and observed via SEM.

2.8. Immunofluorescence cell culturing

Murine L929 fibroblasts and SAOS-2 osteoblasts were cultured in DMEM, Gibco® with 10 % FBS, Gibco® and 1 % ciprofloxacin (Sigma, St. Louis, MO, USA) at 37°C in a humidified condition with 5 % CO_2 and 95 % air. The cells were used after two consecutive passages.

2.9. Fluorescence staining

Cells were seeded onto the 24-well polystyrene cell culture plate, at a density of 5×10^3 cells/well in a humidified condition with 5 % CO_2 and 95 % air for 48 h. Simultaneously, the eluates from different samples were prepared using $1 \text{ cm}^2/\text{mL}$ and maintained in agitation for 24 h in DMEM with 5 % FBS and 1 % ciprofloxacin, respectively. Then, the conventional media was replaced with 500 $\mu\text{L}/\text{well}$ of each eluate from phosphorylated BC, phosphorylated BC + TATT, phosphorylated BC + TiBALDH and control (cells maintained only with conventional media) for 48 h at the same temperature and CO_2 described above. Afterward, the eluates were removed and the wells were washed with 0.01 M PBS (300 $\mu\text{L}/\text{well}$) and then cells were fixed with 3 % glutaraldehyde (300 $\mu\text{L}/\text{well}$) for 30 min at 4°C . The cells were washed again with 0.01 M PBS (three times) and treated with 0.1 % Triton X-100 (300 $\mu\text{L}/\text{well}$) for 5 min at room temperature. After incubation, the wells were washed again, and the cells were incubated with phalloidin-iFluor 488 (1 $\mu\text{g}/\text{mL}$) in 0.01 M PBS and 1 % of Bovine Serum Albumin (BSA) for 1 h at 37°C . Simultaneously the wells were incubated overnight with Rabbit Recombinant Monoclonal anti-Collagen I conjugated to Alexa Fluor® 594 (1:200) and Rabbit Recombinant Monoclonal anti-Fibronectin conjugated to Alexa Fluor® 555 (1:200) at 4°C using the same diluent solution (0.01 M PBS/1 % BSA). Finally, the wells were washed again (three times) and maintained in a solution of 0.01 M PBS and 1 % BSA. Immunofluorescence images were acquired using the Zeiss LSM800 Confocal Fluorescence Microscope. Objective lens: 40x/1.4 NA. Excitation wavelengths: 488 nm for phalloidin-iFluor 488, 594 nm for Alexa Fluor® 594 (Collagen I), and 555 nm for Alexa Fluor® 555 (Fibronectin). Emission wavelengths: 505–550 nm for phalloidin-iFluor 488, 610–650 nm for Alexa Fluor® 594, and 570–620 nm for Alexa Fluor® 555. Image resolution: 1024×1024 pixels with 8-bit depth to ensure high image quality.

2.10. Quantitative measurement of fluorescence intensity

Fibroblast and osteoblast cells were initially seeded in 96-well plates at a density of 5×10^3 cells. The cells were cultured in DMEM with 5 % FBS and 1 % ciprofloxacin and incubated at 37°C in a humidified atmosphere with 5 % CO_2 . After 24 h, the conventional medium was replaced with eluates from phosphorylated BC, phosphorylated BC +

TATT, and phosphorylated BC + TiBALDH. The culture medium was replaced with the corresponding eluates every two days for a total culture duration of 7 days. After 7 days, the eluates were carefully removed, and the cells were washed three times with 0.01 M PBS/1 % BSA to remove any residual media or eluates. The cells were then fixed by incubating with 3 % glutaraldehyde for 30 min at 4°C . Following fixation, the cells were washed again and permeabilized using 0.1 % Triton X-100 in PBS/1 % BSA for 5 min. Subsequently, the cells were incubated with the fluorescence markers, phalloidin-iFluor 488 (1 $\mu\text{g}/\text{mL}$) for 1 h at 37°C , and Rabbit Recombinant Monoclonal anti-Collagen I conjugated to Alexa Fluor® 594 (1:200) and Rabbit Recombinant Monoclonal anti-Fibronectin conjugated to Alexa Fluor® 555 (1:200) overnight at 4°C , following the protocol described above. The fluorescence intensity was quantified using the FLUOstar Omega Microplate Reader. Each well was scanned for fluorescence at the specific excitation and emission wavelengths corresponding to the fluorophores used. This assay was performed in two independent experiments.

3. Results

3.1. Bacterial nanocellulose

The original BNC was proved to be a chemically and thermally robust material. For its morphological characterization of BNC by AFM and surface roughness, please see Fig. S2-S5. The degradation profile of the BNC membranes by TGA showed three mass-loss steps (see Fig. S16). The first thermal stage that constituted a mass loss of 10.8 % was associated with water release between 30 and 100°C . The second step was more pronounced and occurred in $\text{Tonset} = 240^\circ\text{C}$ with 12 % mass loss and $\text{Tmax} = 328^\circ\text{C}$, could be attributed to cellulose degradation, including depolymerization and decomposition of glucose units. The third step represented the degradation of carbonaceous residues that extends from 400 to 600°C with a percentage of residual at 600°C determined was 8.6 %. These results are in good agreement with generally observed thermal behavior of nanocellulose (Gan, Sam, Abdullah & Omar, 2020).

The solid state ^{13}C NMR spectra showed in Fig. S17 reveal distinct signals corresponding to the carbon atoms within the carbohydrate segment of the cellulose structure. Specifically, the signal at δ 104.91 ppm is attributed to carbon C1, while the signal at δ 88.86 ppm corresponds to carbon C4. The region between δ 84–71 ppm (83.50, 74.31 and 71.38) encompasses signals from carbons C2, C3, and C5, and the signal at δ 65.08 ppm represents carbon C6 (for details, please, see Supplementary materials). The degree of polymerization (DP) of BNC determined through viscometry was found to be 2800 (Supplementary materials Table S4), corresponding to an average molecular weight of $453.600 \text{ g mol}^{-1}$.

3.2. Phosphorylation

We confirmed the surface of dried BNC was successfully phosphorylated using a combination of Energy Dispersive X-ray scattering (EDS), conductometric titration and attenuated total reflection fourier transform infrared spectroscopy (ATR-FTIR). In EDS an increase in At% P could be measured as the reaction progresses, to around 3.3 At% P after 40 min. Using ATR-FTIR we could observe the evolution of several peaks with time (Fig. 1, right, Fig. S12), most notably around 825 cm^{-1} , 930 cm^{-1} and 1230 cm^{-1} . Additional peaks that may be related to the introduction of phosphorus appeared around 500 cm^{-1} and very diffused around $2700\text{--}2750 \text{ cm}^{-1}$ (Thomas & Chittenden, 1964a; Thomas & Chittenden, 1964b). To quantify the phosphate content conductometric titrations were performed under the assumption that only the monophosphate-cellulose ester (Cell-O- PO_3H_2) had formed. Under this assumption the reaction order appears to be pseudo-first order with a rate of 0.057 min^{-1} with a final phosphorylated degree of 2.7 mmol/g (Fig. 1, left). Due to the brittle nature of the BNC membranes after

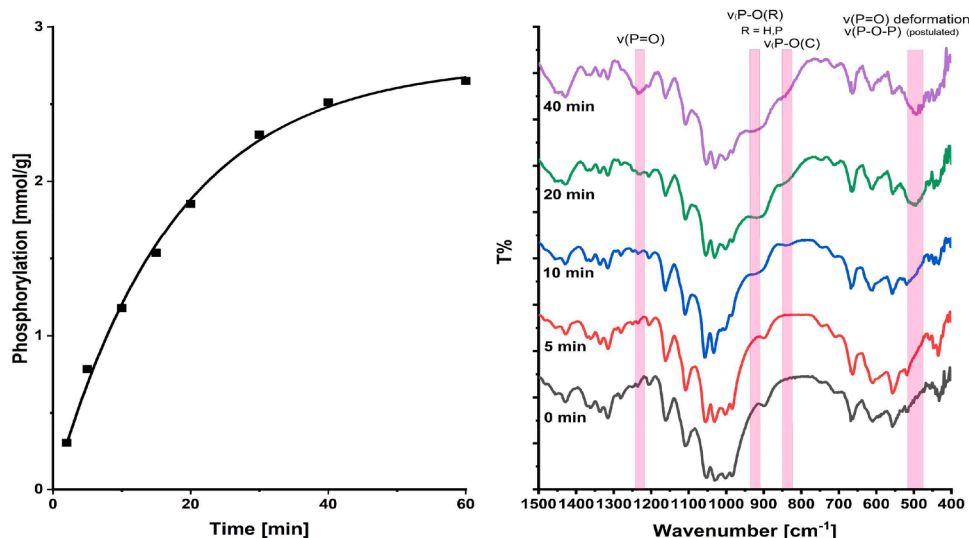


Fig. 1. Phosphorylation degree in mmol/g as a function of time for Dry Bacterial nanocellulose (■) (Left) ATR-FTIR spectra of the evolution of phosphorus related IR-peaks as a function of time. Pristine BNC (black), 5 min (red), 10 min (blue), 20 min (green) and 40 min (purple).

prolonged heating, subsequent samples were prepared using 20 min as a time point, yielding 1.5–1.8 mmol/g of phosphate.

3.3. Fiber morphology

3.3.1. Pristine dried bacterial nanocellulose

The provided dried BNC exhibits a surface morphology (Fig. 2A) consisting of long ($>1\mu\text{m}$), thin (64.9 ± 13.0 nm) twisted fibres of several micrometres in length with a large aspect ratio, which in many places are interwoven to form a fibrous mat. Allowing the sheet to swell in ultrapure water for seven days (Fig. S3 C,D) the fibres swell to 70.9 ± 12.4 nm, a 9 % increase. Treating the dried BNC with 0.1 M HCl over seven days changes the morphology, smaller crystallites appear on the surface with the overall fibre outline being maintained (Fig. S3 A,B). The fibre outline itself reduces in size to an approximate 50.9 ± 13.9 nm, with the smaller crystallites present on the surface having an approximate width of 22.3 ± 5.3 nm. When treated with 0.1 M NaOH, much of the original fibre structure is retained, with a decrease in fibre size to 60

± 12.4 nm (Fig. S3 E,F).

3.3.2. Phosphorylation of dried bacterial nanocellulose

After phosphorylation of dried BNC the surface becomes more porous on the microscale compared to pristine bacterial nanocellulose (Fig. 2B). Treatment with urea had a limited effect on surface morphology (Fig. S9). After phosphorylation the fibres retain much of their original shape and size, consisting of fibres twisted together with a minor increase in fibre diameter to 65.7 ± 12.8 nm. When stored for seven days in ultrapure water (Fig. S7, C,D), the distance between fibres increases, opening up the surface of the material. A closer examination show that the fibre morphology itself has changed, appearing notably more ribbon-like than freshly prepared phosphorylated BNC, with an average width of 68.9 ± 14.2 nm on the thinner edge of the fibres (Fig. S4, A,B). Storing the phosphorylated sheets under very acidic conditions in 0.1 M HCl resulted in the distance between fibres increasing compared to ultrapure water (Fig. S6, A,B). Opening up the

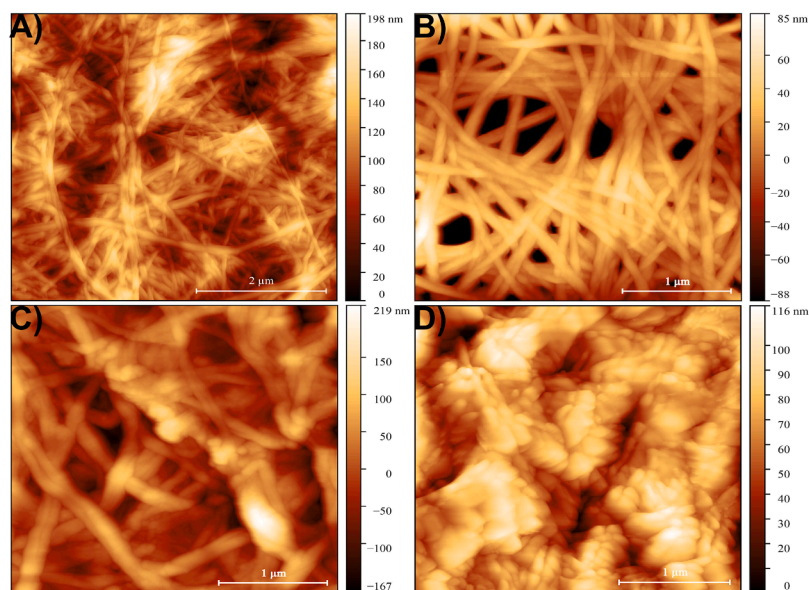


Fig. 2. AFM images of Bacterial nanocellulose Sheet as is (A $5 \times 5 \mu\text{m}$), phosphorylated BNC (B, $3 \times 3 \mu\text{m}$), phosphorylated BNC coated with pre-formed colloidal TATT (C, $3 \times 3 \mu\text{m}$), phosphorylated BNC- modified by TiO_2 derived from TiBALDH® (D $3 \times 3 \mu\text{m}$).

structure to such an extent as to be reminded of supercritically dried BNC (Fig. S8) The phosphorous content decreased from 2.2 At% P in ultrapure water to 1.0 At% when stored under very acidic conditions. The HCl treated phosphorylated sample (Fig. S4, A,B) exhibits a ribbon-like structure with the fibre width decreasing to 63.5 ± 17.8 nm. Storing under basic conditions in 0.1 M NaOH, resulted in the formation of large several micrometer gaps between well resolved fibres while more commonly fibre clusts appear so dense as to be poorly resolved (Fig. S7, E,F). Making it difficult to differentiate between individual fibres by SEM. Using AFM the general outline of the original fibres can be seen, with the actual fibre surface containing many globular structures with an approximate dimension of 44.8 ± 9.1 nm (Fig. S4, E,F). Similar to the samples stored under acidic condition, basic conditions also lead to a decrease in phosphorous content. According to EDS the phosphorous content decreased to 1.3 At%.

3.4. Introduction of nano-TiO₂

Treating phosphorylated bacterial nanocellulose with stoichiometric excess of TiBALDH at room temperature results in a loss of the previously observed open surface structure of phosphorylated BNC, in favour of the formation of titania crystallites across the surface. The TiBALDH derived product contains relatively large, aggregated and angular structures of titania across the surface (Fig. 2D, Fig. S5, E,F). The surface titania structures formed by TiBALDH are ca. 5–10 nm in height in the smaller range and up to 25 nm in the larger range. Length wise the particles are variable with some as small as 30 nm, while others are up to 160 nm depending on surface orientation, averaging around 75.4 ± 40.7 nm. EDS data (Fig. S7) confirms the successful introduction of Titania with 1.1 At% Ti and a P:Ti ratio of: 1: 0.45. Treating the phosphorylated bacterial nanocellulose with stoichiometric excess of colloidal TATT lead to uniform coverage of BCN fibres, increasing the fibre thickness from 65.7 ± 12.8 nm in phosphorylated BNC to 71.6 ± 6.6 nm in TATT-covered phosphorylated BNC (Fig. 2C, Fig. S4, G, H). This is to be expected, as the colloid consists of pre-formed hydrated TiO₂ particles, which in principle coordinate to the surface via the introduced phosphate group but may also aggregate or gelate. EDS data (Fig. S8) confirms the successful introduction of Titanium with 1.1 At% Ti and a P:Ti ratio of 1:0.8. Both phosphorylation and introduction of oxide nanoparticles are well reproducible under identified conditions facilitating potential up-scaling and therapeutic use of the material.

3.5. X-ray diffraction

The provided source of cellulose starting material (Fig. S11) was crystalline, presumably largely consisting of cellulose I α (Wada, Okano & Sugiyama, 2001) based on peak shape between 6.5–8 2 θ . The calculated crystallinity was 49.6 % based on peak height and crystallite size of 6.3 nm based on the Scherrer equation. Hydrating pristine dry bacterial nanocellulose in ultrapure water increased the Scherrer crystallite size to 12.6 nm and decreased measured crystallinity to 34.3 %. Hydration of BNC in 0.1 M NaOH resulted in a loss of crystallinity to 26.9 % and an increase in diffraction intensity around 5–6 2 θ . Which corresponds to the calculated 1–10 miller index in cellulose II. Hydrating pristine BNC in 0.1 M HCl increased the crystallinity to 34.8 %. The diffraction pattern of as-synthesized phosphorylated BNC (Fig. S11) is similar to pristine BNC, with a higher calculated crystallinity of 58.9 % and a Scherrer crystallite size of 12 nm. In ultrapure water phosphorylated BNC behaves similarly to pristine BNC, losing some crystallinity (to 33.5 %) and increasing the Scherrer crystallite size to 17 nm. Maintained degree of crystallinity is in favor of unchanged mechanical properties such as brittleness, crucial for up-scaling and further practical use of the material. When placed in either 0.1 NaOH or HCl, there is a large change in peak ratio between 6.5–8 and 10.4 2 θ . Due to the overlap between the most intense diffraction peaks of cellulose and anatase titania samples were sintered to confirm the presence of TiO₂

(Fig. S12). After sintering at 600 °C only 7.5 wt% white residue remains of the TiBALDH modified material and 14.5 wt% white residue remains for the TATT modified material. Sintering the material at 500 °C indicates the presence of anatase titania (Fig. S12) together with some residue (turning the material brown). The remaining residue had Scherrer crystallite sizes of 19.8 nm for TiBALDH and 32.2 nm for TATT.

3.6. Tetracycline desorption

The nanocomposite derived from TiBALDH displayed adsorption of 41.4 ± 4.8 mg of tetracycline per g of cellulose dressing. The appearance of two additional shoulder peaks at 1600 cm⁻¹ and 1580 cm⁻¹ in transmission FTIR (Fig. S13) can be attributed to the inclusion of chemically bound tetracycline (Myers, Tochon-Danguy & Baud, 1983). The nanocomposite material released 30.8 ± 2.9 % tetracycline after 5 h, reaching 53.3 ± 2.9 % tetracycline release after 120 h. The TATT derived composite had 46.5 ± 2.2 mg g⁻¹ tetracycline absorbed per g of cellulose dressing. The TATT nanocomposite released 39.4 ± 0.2 % tetracycline after 5 h in desorption medium, reaching up to 61.4 ± 1.7 % after 120 h (Fig. 3)

3.7. Cell assays

As the surface modification of the BCN is intended for use in wound dressing materials, it is of paramount importance to test the cytotoxicity. In addition, pseudo-wound healing and cell adhesion assays provide additional insight into the suitability of the material and subsequent modifications for wound healing. The samples in Table 1 were evaluated.

3.7.1. Cytotoxicity assay

Given the worldwide concerns regarding nanotoxicity in biomaterials, the potential cytotoxic effects of TiO₂ nanoparticles covered BNC was investigated. Most functionalized BNC films showed atoxicity for both cell lines, maintaining cell viability above 85 % (Fig. 4, Table 1). Both high (1) and low (2) phosphate content BNC samples showed no decrease in cell viability for L929 Murine Fibroblasts. High phosphate content BNC did slightly decrease in cell viability for SaOS-2 osteoblastic cells. After covering phosphorylated BNC with TiO₂, both “bare” (11) and lactate covered (10) TiO₂ maintained cell viability close to 100 % for both fibroblasts and osteoblastic cells. Covering the TiO₂ with antibiotic tetracycline induced a decrease in cell viability for TATT covered (31) BNC, but not TiBALDH (30). After desorption of tetracycline in citrate buffer, cell viability for TiBALDH covered (33) BNC decreased slightly. Cell viability for TATT covered BNC (32) remained the same after desorption. In contrast to the previous samples, BNC/TiBALDH/AgNO₃ (34) showed cytotoxicity effect with a significant decrease in fibroblast (below 65 %), while the viability of osteoblastic cells reduced drastically, reaching 100 % cell death against samples 34 and 35 (cotton nanocrystals/TiBALDH/AgNO₃).

3.7.2. Evaluation of pseudo-wound closure

Previous studies have demonstrated that BC exhibits remarkable wound healing properties due to its unique physicochemical and biological characteristics. The 3D-dimensional network structure of BC effectively allows normal gas and liquids exchange, which is essential for proper wound treatment. BC also serves as an ideal carrier for the slow release of drugs, further enhancing wound healing and promoting skin tissue regeneration. Its high water absorption and retention capabilities enable efficient management of wound exudates, while its mechanical strength provides skin protection. Additionally, makes it suitable for dressing irregularly shaped wounds, as well as allows easy wound inspection due its translucency property (Wahid et al., 2021). Khalid et al. (Khalid et al., 2017) reported that BNC/TiO₂ biocomposites notably accelerated wound closure by *in vivo* model, with wound area reduction observed from 289 mm² on day 0 to 86 mm² on day 15 in the treated

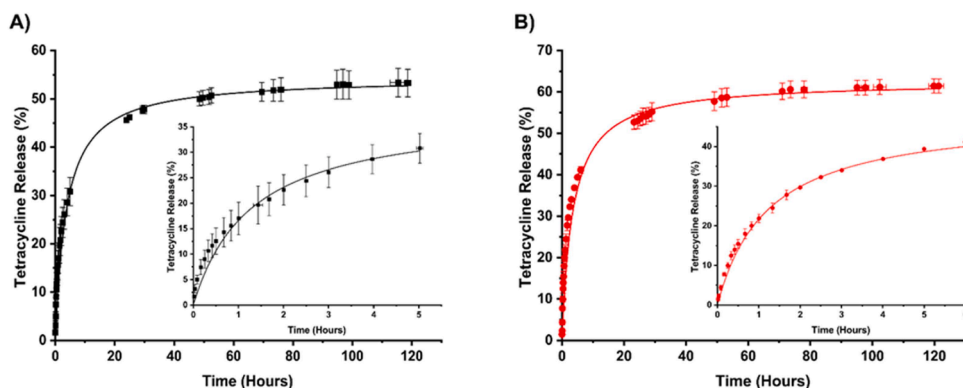


Fig. 3. Desorption of the broad-spectrum antibiotic Tetracycline from phosphorylated bacterial nanocellulose sheets covered by TiO₂ derived from TiBALDH (left, black) and colloidal triethanolamine terminated TiO₂ (right, red). Fitted with non-linear 2nd order fitting in origin.

Table 1

Samples tested for cytotoxicity, pseudo-wound healing and cell adhesion assays.

Sample number	Nomenclature
1	BNC-PO ₄ ~2.7–4 wt%
2	BNC-PO ₄ ~0.5–1.5 wt%
10	BNC-PO ₄ - TiBALDH
11	BNC-PO ₄ - TATT
30	BNC-PO ₄ - TiBALDH + tetracycline
31	BNC-PO ₄ - TATT + tetracycline
32	dry BNC-PO ₄ - TATT + tetracycline after desorption in citrate buffer
33	dry BNC-PO ₄ - TiBALDH + tetracycline after desorption in citrate buffer
34	BNC wet membrane + 10 mol % 2:1 TiBALDH: AgNO ₃
35	Cotton cellulose nanocrystals + 10 mol% 2:1 TiBALDH:AgNO ₃

group. In comparison, wounds treated with pure BC or a negative control showed significantly slower closure rates. These findings suggest that the incorporation of TiO₂ nanoparticles in BC significantly enhances its healing potential, likely by supporting fibroblast function and tissue remodeling in the wound area. Similarly, phosphate-crosslinked BC-based hydrogels also play a vital role in osteogenic as shown by Suneetha and collaborators (Suneetha, Kim & Han, 2024).

In this work (Fig. 5) the samples 2, 10, 11 and 30 had a positive effect on L929 cell migration, enabling 100 % pseudo-wound closure within 24 h as well as the positive control (only culture media) Samples 31, 33 and 34 demonstrated a negative effect on cell migration for L929 cells. For SaOS-2 cells, samples 10 and 33 promoted pseudo-wound closure within 24 h as well as the positive control. Sample 34 had a negative effect, preventing pseudo-wound closure within the analysis

timeframe. The micrographs showing the closure of the pseudo-wounds over 48 h can be observed in Fig. S2.

3.7.3. Cell adhesion assay

Data indicate that all tested samples of BNC-PO₄ (samples 1,2) and BNC-PO₄-TiO₂ composites (samples 10, 11) analyzed supported the attachment, cell adhesion, and proliferation of both cell lines (Figs. 6 and 7). Moreover, high cell spreading and a fully developed cytoskeleton were visible. Similar results were reported by Khan et al. (Khan et al., 2015), who demonstrated that regenerated BC (RBC)-TiO₂ nanocomposites exhibited excellent cell adhesion and proliferation capabilities with animal fibroblast cells, without showing any toxic effects.

3.7.4. Fluorescence staining

During cell migration, the cell initially extends protrusions, such as lamellipodia and filopodia, establishes adhesion points, and ultimately retracts its tail. The actin cytoskeleton plays a central role in this process (Le Clairche & Carlier, 2008; Gardel, Schneider, Aratyn-Schaus & Waterman, 2010). Moreover, type-I collagen and fibronectin are two critical extracellular matrix (ECM) components that significantly contribute to healing and tissue regeneration (Kanta, 2015). Type-I collagen, the most abundant ECM component provides a scaffold that binds other proteins and proteoglycans, facilitating cell interaction. Additionally, fibronectin plays a pivotal role in controlling cell adhesion, spreading, migration, proliferation, and differentiation, further highlighting its importance in tissue repair and regeneration (Parisi et al., 2020).

In the present study, confocal immunofluorescence analysis was used to visualize the F-actin, type I collagen and fibronectin biomarkers in fibroblast and osteoblast cells of different treatment group. Our findings indicated that biomarkers expression was observed in both cell lines

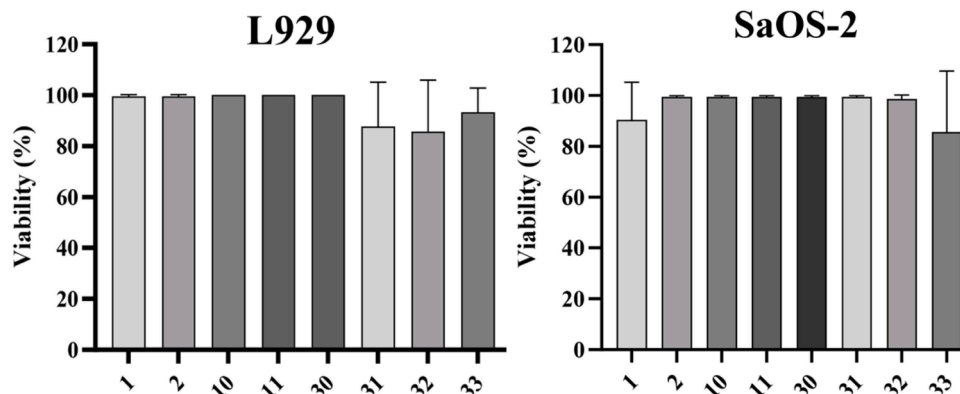


Fig. 4. Viability of L929 and SaOS-2 cells upon contact with eluates from the functionalized BNC samples.

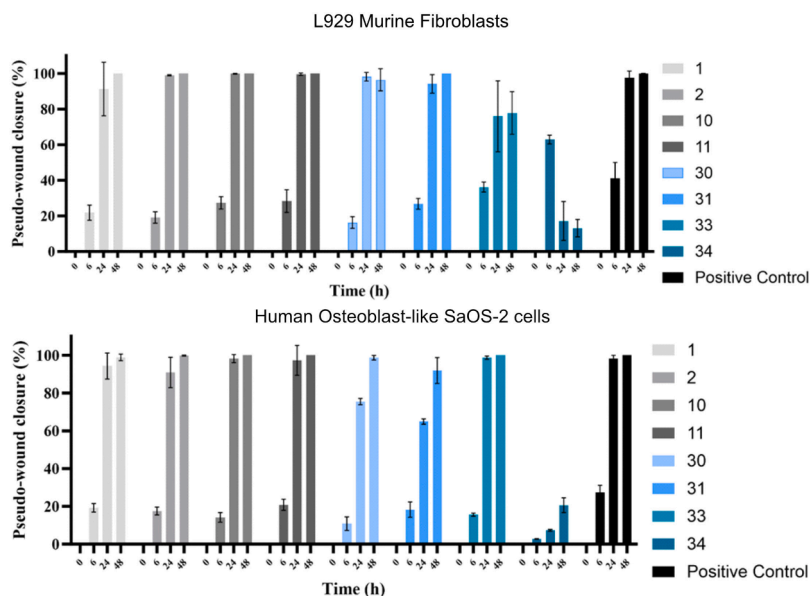


Fig. 5. Effect of different functionalized BNC composites on migration of L929 and SaOS-2 cell lines by evaluation the pseudo-wound closure at times of 0, 6, 24 and 48 h.

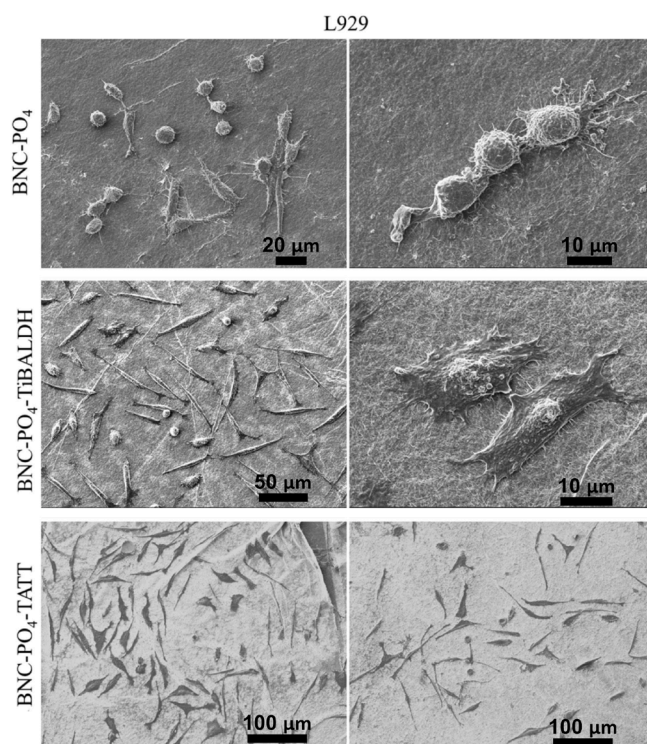


Fig. 6. L929 cells adhered on different functionalized BNC composites after 72 h of incubation.

following exposure to BNC-PO₄ composites for 7 days as shown in Figs. 8-10.

3.7.5. Quantitative measurement of fluorescence intensity

Our results involving fluorescence intensity quantification showed a significant increase in F-actin expression in L929 fibroblasts and SaOS-2 osteoblasts treated with the BNC-PO₄ group compared to BNC-PO₄-TATT, BNC-PO₄-TiBALDH and control (Fig. S15). The expression of fibronectin was significantly higher than type-I collagen, although no

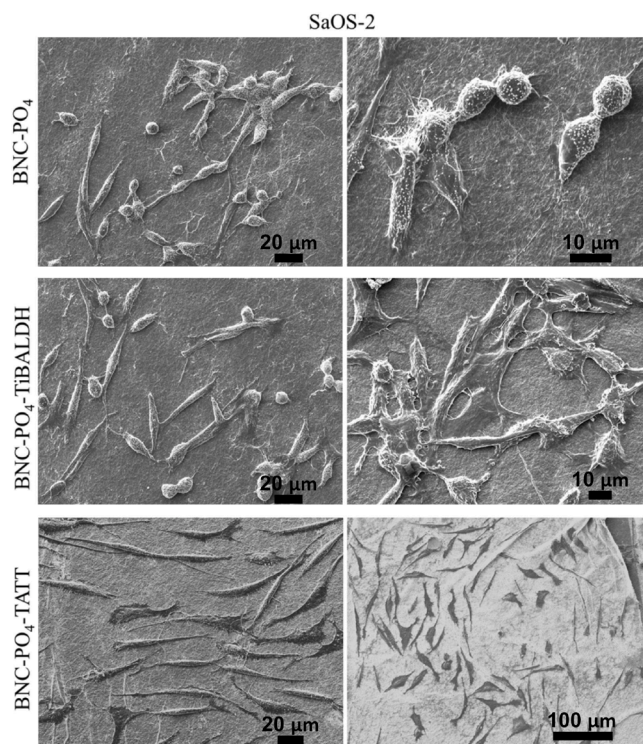


Fig. 7. SaOS-2 cells adhered on different functionalized BNC composites after 72 h of incubation.

significant difference in their expression were observed between the different experimental groups. It is important to mention that both cell lines treated with eluates from BNC-PO₄ composites were exposed to a culture medium containing only 5 % FBS, while the control cells received 10 % FBS. This suggests that TiO₂ nanoparticles (TiBALDH and TATT) positively influenced the expression of biomarkers investigated. Nevertheless, further molecular quantification assays and *in vivo* model studies would be beneficial to confirm the relevance of these inorganic particles in enhancing the expression of protein and cytoskeletal markers and their contribution to tissue regeneration.

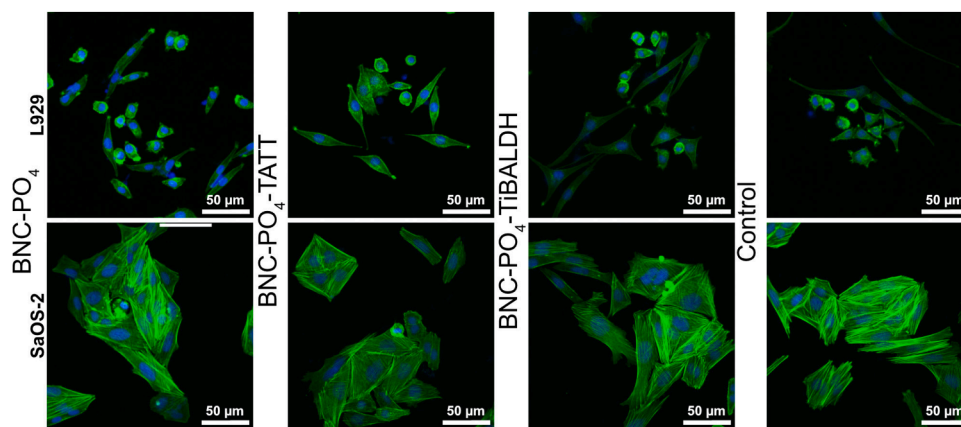


Fig. 8. Confocal imaging of murine L929 fibroblasts and SaOS-2 osteoblasts: F-actin (green) was labeled with phalloidin-iFluor 488 (green), and the nuclei (blue) counterstaining with DAPI. Fluorescence staining of the actin cytoskeleton was registered on fibroblasts and osteoblasts cultured for 7 days with different eluates from BNC-PO₄, BNC-PO₄-TATT and BNC-PO₄-TiBALDH. Control cells was maintained with only conventional media.

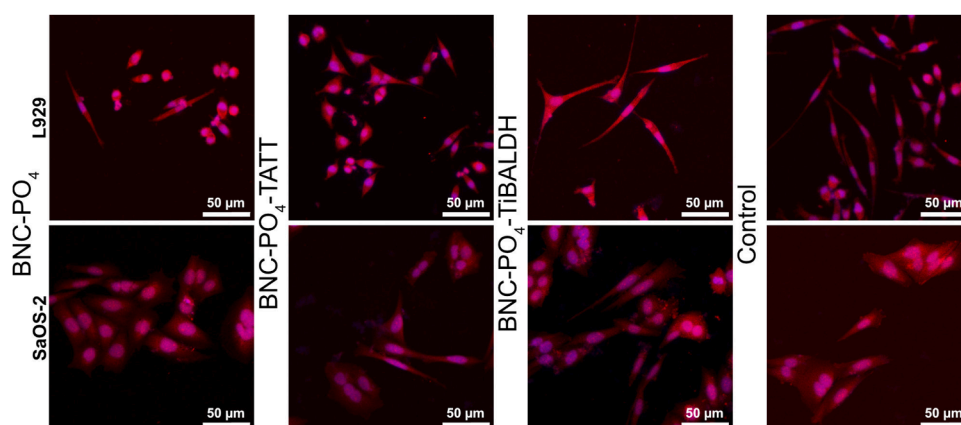


Fig. 9. Confocal imaging of murine L929 fibroblasts and SaOS-2 osteoblasts: Type I-Collagen (red) was labeled with Rabbit Recombinant Monoclonal anti-Collagen I conjugated to Alexa Fluor® 594 and nuclei counterstaining with DAPI (blue). Fluorescence staining of collagen Type I was registered on fibroblasts and osteoblasts cultured for 7 days with different eluates from BNC-PO₄, BNC-PO₄-TATT and BNC-PO₄-TiBALDH. Control cells was maintained with only conventional media.

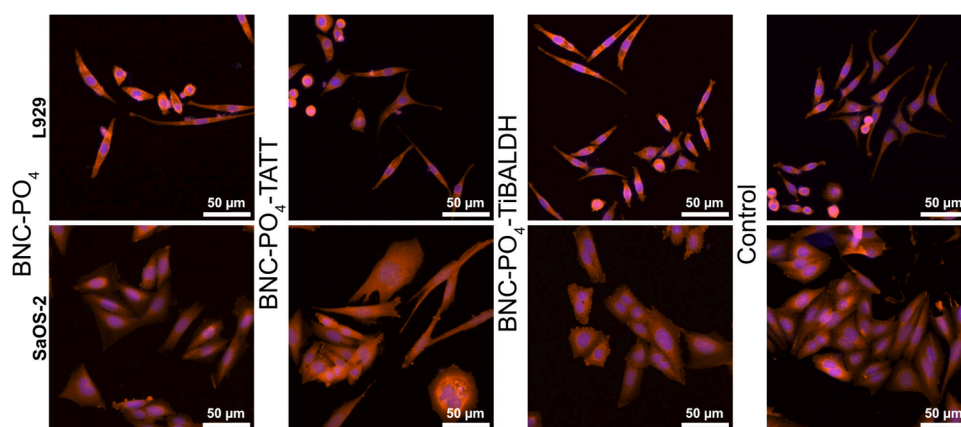


Fig. 10. Confocal imaging of murine L929 fibroblasts and SaOS-2 osteoblasts: fibronectin (red) was labeled with Rabbit Recombinant Monoclonal anti-Fibronectin conjugated to Alexa Fluor® 555 and nuclei counterstaining, with DAPI (blue). Fluorescence staining of fibronectin was registered on fibroblasts and osteoblasts cultured for 7 days with different eluates from BNC-PO₄, BNC-PO₄-TATT and BNC-PO₄-TiBALDH. Control cells was maintained with only conventional media.

4. Discussion

4.1. Phosphorylation

Phosphorylation of cellulose is an ester-forming reaction, which the surface cellulose molecules easily undergo in acidic medium (Inagaki, Nakamura, Asai & Katsuura, 1976). It forms a C—O—P bond on the surface polymer molecule, leaving 3 oxygen atoms bound to phosphorus for potential surface complexation to metal oxide nanoparticles. Titania nanoparticles should be strongly bound to such modified matrix, otherwise titania is washable due to the poor affinity between titania and cellulose, leading to the release of nanoparticles in the wound environment. As titania has excellent affinity for phosphate, forming a hydrolytically stable M—O—P bond, we decided to introduce phosphate onto the surface. As described in Section 3.1, phosphorylation was confirmed a variety of techniques, however the aforementioned EDS (on carbon tape) and FTIR analysis were difficult to quantify reliably and so the BNC surface phosphorylation degree was determined conductometrically by measuring the equivalent base consumption of the material after converting to the acid form. A large increase in hydroxide consumption was observed with increase in reaction time, corroborating EDS and FTIR results regarding successful phosphorylation. The reaction itself proceeded smoothly, though the amount of phosphate present has been noted to vary between experiments depending on the remaining surface-adhered liquid and shape of crucible used, with wider crucibles being favoured. Presumably because the increase surface area promotes evaporation of water, allowing adequate reaction temperatures to be reached more readily. It should be noted that the bacterial nanocellulose films became increasingly brittle with increase of reaction duration. Due to the increased brittleness, an intermediate time point of 20 min was chosen for subsequent samples as a compromise between material flexibility and phosphorylation degree.

4.2. Fiber morphology

4.2.1. Pristine dried bacterial nanocellulose

Bacterial nanocellulose (BNC) differs considerably from other types on nanocellulose. It is set apart from other cellulose sources such as vegetal cellulose by the long, interwoven microfibrils, which can be produced without the need for extensive mechanical or chemical treatment in order to obtain high-purity cellulose. It is naturally produced as a biofilm by bacteria with minimal side products, and as such, it retains most of the original morphology after purification. When freshly produced it exists as a hydrogel which can be treated further or like the commercial wound dressing used here, it can be compressed and dried as a film. Presented in its dried state, this particular cellulose source appeared to consist of long twisted fibres of several micrometres in length, forming a fibrous mat of cellulose. The constituent BNC fibres swell up after several days in water. Storage under very acidic conditions made small crystallites appear on the surface together with a reduction in fiber thickness. This is expected as cellulose, in particular the amorphous regions of cellulose present on the surface, is known to hydrolyse in acidic environment. The fibres maintained much of their original structure when treated with lye, though a small decrease in fibre width was noted. This may be due to partial base hydrolysis of cellulose, minor surface regeneration or due to selection bias as only fibres with clearly demarcated borders are chosen. It is noted that some regions on base-treated dried bacterial nanocellulose appear more globular compared to the original bacterial nanocellulose, supporting the notion that the cellulose surface packing has changed to some extent.

4.2.2. Phosphorylation of dried bacterial nanocellulose

Surface charge, charge repulsion / hydrogen bonding between fibres plays an important role in the overarching morphology of materials and it was observed that the morphological changes may be attributed to the introduction of the phosphate group. As seen in Section 3.2.2, the

observed surface structure of phosphorylated BNC strongly depended on pH storage conditions. Hydrating the materials for a prolonged period of time in ultrapure water changed the appearance of the fibres to become noticeably more ribbon-like. These ribbon-like fibres appeared at least partly folded, which made it difficult to measure an accurate width. When comparing the HCl treated phosphorylated BNC and HCl treated pristine BNC there is a noticeable difference in surface structure. In pristine BNC there are clearly observable small nanocrystalline domains distributed across the fibre surface, which are not present on phosphorylated BNC. Storage under basic conditions led to the formation of globular structures on the surface of the previously observed smooth ribbons. This could be due to cellulose regeneration, the negative surface charge of the phosphate group under strongly high alkaline conditions or another mechanism. The observed decrease in phosphorus content upon treatment with acid or base indicate that the cellulose-O-phosphate bond is liable to (partial) hydrolysis, being more sensitive to acidic conditions. The morphological changes of the material upon phosphorylation and pH treatment are notable; comparing the pristine BNC sheets with phosphorylated BNC, the surface becomes more porous upon phosphorylation and strongly influenced by pH with different morphologies present depending on storage conditions (Patoary, Farooq, Zaarour & Liu, 2021). Dried phosphorylated cellulose is a brittle material, which may pose difficulties in up-scaling of the phosphorylation process. However, if then the ready composite is kept in humid conditions this challenge can be avoided in therapeutic applications.

4.3. Introduction of nano-TiO₂

Nanosized titanium dioxide is an easily produced and up-scaled material. It is generally considered to be biocompatible and antibacterial. Depending on the surface chemistry of the TiO₂ nanoparticles involved, it may induce blood coagulation however, which may be undesirable for some applications (Svensson et al., 2021). To test the viability of the material, two versions of BNC-PO₄ – Titania composites were prepared using TiBALDH and TATT respectively. TiBALDH is a water-soluble precursor to nano-sized titania. It exists in solution equilibrium with ammonium tris-lactato-titanate (NH₄)₂[Ti(Lactate)₃] and uniform, crystalline, anatase titania which is stabilized by surface-capping with lactate (Groenke et al., 2012). This equilibrium can be shifted by change in solvent polarity, addition of salts or as used here, a strongly competing ligand, which shifts the equilibrium towards lactate-capped nano-Titania. TATT by comparison is a colloidal suspension of anatase titania, with an amorphous hydrated surface and crystalline anatase core. TATT is made via the controlled hydrolysis of a titanium alkoxide precursor in the presence of a surface capping agent (Kessler, Seisenbaeva, Håkansson & Unell, 2008). The introduction of a chelating ligand to the metal alkoxide sol leads to the formation of self-assembled micellar aggregates during hydrolysis/polycondensation. These micelles templated by self-assembly of ligands (MTSALs) are covered by residual ligands (Kessler et al., 2006), which in the case of TATT has been charged under acidic conditions to provide a charge stabilized colloid with particles in the range of 3–4 nm (Kessler, Seisenbaeva, Håkansson & Unell, 2008). In aqueous media the capping agent is hydrolysed to form a basic suspension of negatively charged colloidal, bare TiO₂ which binds to the surface via coordination with the introduced phosphate group. With TATT, there is a noticeable difference in surface morphology compared to TiBALDH. This can readily be observed as the original fibre morphology appeared to be largely preserved. The increase in observed fibre thickness corresponds to the size of two particles, indicating full coverage of the phosphorylated BNC fibres by TATT. The difference in P:Ti ratio observed here is most likely due to the alkaline hydrolysis of phosphate which was previously observed with phosphorylated BNC.

4.4. X-ray diffraction

It should be clearly noted the instrument used a Mo-source ($K\alpha = 0.7093 \text{ \AA}$) instead of a Cu-source ($K\alpha = 1.5406 \text{ \AA}$). Leading to a loss in angular resolution due to contraction of the diffraction pattern towards lower Bragg angles. Due to the lower angular resolution, idealized powder pattern only have a 69.5CI% based on peak height. Thus, CI% in Section 3.4 would be underreported. The observed decrease in crystallinity and increase in Scherrer crystallite size for pristine BNC was presumably due to the swelling and hydration of the cellulose fibres. In ultrapure water BNC-PO₄ behaves similar to the pristine material, with a loss in crystallinity and increase in Scherrer crystallite size. Placing the material in either acidic or basic environment causes a change in peak ratio between the diffraction at 6.5–8 and 10.4 2 θ , indicating that the packing of the material has changed. This implies that the pH not only affects the overall morphology of BNC-PO₄ as mentioned in 4.2.2 but the crystal packing of the cellulose fibres itself is also influenced by pH after phosphorylation.

4.5. Tetracycline desorption

Environmental effects of presently used paradigm of systemic antibiotic drug treatment are associated with release of residual medicines not consumed by the body into the wastewater. This leads to dangerous increase in antibiotic pollution in ground waters and water bodies, resulting in emerging multi-resistant pathogens (Larsson & Flach, 2022). An alternative to the systemic treatment is the topical one is permitting to safely dispose the residual pharmaceutical bound to an applied carrier material. The release of many pharmaceuticals from nanocrystalline cellulose and derived composites is, however, quite rapid. Thus, to delay drug release, cellulose has been modified as described in Section 4.1-4.2.3 and nano-sized titania (TiBALDH / TATT) introduced onto the surface. The surface chemistry between titania sources is notably different, TiBALDH-derived titania is presumed to have a surface capping of lactate, which coordinates quite strongly to titania via chelation with both lactate hydroxide and carboxylate groups (Groenke et al., 2012). Thus, any pharmaceutical that is to be chemisorbed onto the surface will be competing against surface bound lactate. TATT by comparison contains a surface capping which in theory hydrolyses in water to provide a bare titania surface. Thus, pharmaceuticals should be able to be chemisorbed onto the surface without any direct competition with other ligands. For drug ad-/desorption studies the drug tetracycline was chosen as it is a broad-spectrum antibiotic with oral and topical applications. In addition, it is a drug, which can be readily measured by UV-VIS due to its characteristic absorption in the range of 300–400 nm. For both sources of titania, when measuring tetracycline desorption, the nanocomposite materials appeared to release tetracycline quite slowly, which is beneficial for sustained drug release. The TATT derived composite had a slightly greater amount of tetracycline adsorbed. This is presumably due to the greater TiO₂ content in the TATT derived composite (7.5 wt% vs 14.5 wt%). The kinetics behind tetracycline desorption from both composites appeared to follow 2nd order kinetics. Indicating that the release of tetracycline is most likely dependent on the concentration of two reactants. Assuming TiO₂ in the solid state doesn't play a significant role one can assume the desorption in part relies on the concentration of desorption media itself, which in this case citrate buffer. The other component would naturally be the concentration of tetracycline in solution.

4.6. Cell assays

4.6.1. Cytotoxicity assay

A preliminary cytotoxicity assay is one of the most important evaluations of the biological properties of the biomaterials prior to *in vivo* assessment. According to the ISO 10,993–5, if the cell viability is greater than 70 %, then the material is considered as non-cytotoxic. Cell

viability of L929 and SaOS-2 was assessed in section 3.6.3 by MTT assay. It was found that of the examined pristine, phosphorylated and TiO₂ covered materials, none of the functionalized BC films showed cytotoxicity for both cell lines.

However, while the cytotoxicity assay indicated no significant toxicity for the materials *in vitro* (See Table S5) it is important to highlight the potential risks TiO₂ nanoparticles, particularly regarding their cytotoxicity and effects *in vivo* (Ayorinde & Sayes, 2023; Skocaj, Filipic, Petkovic & Novak, 2011; Zhangjian Chen et al., 2020). While some studies highlight their antimicrobial and anti-inflammatory properties in scaffolds and wound dressings, their potential to induce oxidative stress cannot be overlooked, as this biological effect can lead to DNA damage and mitochondrial dysfunction. Toxicological studies on nano-TiO₂, encompassing acute, subacute, subchronic, and chronic oral exposure, provide critical insights into their safety profile. Although acute toxicity studies generally indicate low toxicity, prolonged exposure can elicit significant biological effects, influenced not only by nanoparticle size but also by surface charge and aggregation state. Subacute and subchronic studies have reported potential bioaccumulation, oxidative stress, and inflammatory responses, particularly in the liver, kidneys, and gastrointestinal tract. Chronic exposure raises concerns regarding long-term systemic effects, including metabolic disturbances and potential carcinogenicity (Zhangjian Chen et al., 2020).

Nevertheless, several studies, including the present one, have focused on functionalization and doping strategies to mitigate these adverse effects while maintaining well-established biological properties. A deeper understanding of the mechanisms underlying nano-TiO₂ cytotoxicity, incorporating advanced molecular and omics-based approaches, is crucial for defining safe exposure limits in medical and industrial applications (Zhangjian Chen et al., 2020).

4.6.2. Evaluation of pseudo-wound closure and cell adhesion assay

Cell migration is a rate-limiting event during the wound-healing process to re-establish the integrity and normal function of tissue layers after injury. The principle of the method used is based on the creation of a 500 μm gap (pseudo-wound) on a confluent cell monolayer. The cells at the edge of the artificial "wounded" field will start migrating into the cell-free area, forming new cell-cell contacts. For both cell lines (murine fibroblasts and osteoblasts), high phosphate content on BNC (3.6, sample 1) didn't promote migration, however decreasing the phosphate content (3.6, sample 2) had a positive effect on murine fibroblasts. Covering BNC-PO₄ with either TiBALDH (3.6, sample 10) or TATT (3.6, sample 11) had a positive effect on L929 cell migration, enabling full pseudo-wound closure within 24 h, indicating that the material is quite beneficial for wound healing. In contrast, BNC-TATT with tetracycline (3.6, sample 31) appeared to negatively influence wound healing, presumably due to the decrease in fibroblast cell viability observed in section 3.6.1. For osteoblastic SaOS-2 cells, only the TiBALDH-covered BNC (sample 10) provided a positive effect on cell migration, while the other materials, including those containing TATT (sample 11) or BNC-TiBALDH with tetracycline (3.6, sample 31), lost their positive wound-healing effect on osteoblastic cells. Curiously, after tetracycline desorption in citrate buffer, BNC-TiBALDH (3.6, sample 33) displayed a negative effect on wound healing for fibroblasts but a positive effect on osteoblastic cells. Full statistical analysis is provided in Supplementary materials Tables S6-S9.

Adhesion is the first response of the cell when it comes into contact with a biomaterial, and plays an essential role in regulation of the subsequent biological behavior of cells. In the course of the cell adhesion process, cells initially "sediment" to the surface with their spherical bodies. Then, cells "flatten" mostly by nonspecific interactions. If the surface is suitable, cells "fully spread" with focal adhesion maturation and create stable contacts via actin skeleton reorganization to reach their maximum spreading area. Data in section 3.6.3 indicated that all samples analyzed (Section 3.6, samples 1,2, 10, 11) supported the

attachment, cell adhesion, and proliferation for both cell lines. Moreover, high cell spreading and a fully developed cytoskeleton were visible. On the whole, the positive biological outcomes observed for phosphorylated and TiO₂ functionalized-samples indicate promising prospects for diverse applications in tissue engineering.

Similar to established BNC-based dressings such as Membracel®, Nexfill®, Bionext®, and Suprasorb® X + PHMB, which facilitate wound closure by promoting cell migration, tissue regeneration, as well as antimicrobial activity due to the presence of polyhexanide in its composition (Rasouli, Soleimani, Hosseinzadeh & Ranjbari, 2023; Choi et al., 2022, Zahel et al., 2022), the phosphorylated and TiO₂ functionalized BNC also exhibited remarkable potential in promoting murine fibroblast migration, as well as enhancing the spreading, adhesion, and proliferation of both osteoblastic and fibroblastic cells, as indicated by its performance *in vitro* studies. Although further experiments are necessary to confirm these findings *in vivo* models, such as the rat calvaria and skin excision wound models, its inherent antimicrobial, antioxidant, and anti-inflammatory properties, attributed to the incorporation of TiO₂ nanoparticles, emphasize its potential for advanced wound dressings that meet the evolving demands of modern wound care technologies.

4.6.3. Fluorescence staining and quantitative measurement of fluorescence intensity

Functionalized biomaterials incorporating inorganic compounds, such as phosphate groups and titanium oxide nanoparticles, have shown promising effects on the expression of extracellular matrix (ECM) and cytoskeletal biomarkers. These strategies may enhance cellular adhesion, migration, proliferation, and differentiation due to the unique properties of the inorganic particles. Given their range of sizes and high surface area, TiO₂ nanoparticles have been shown to modify the topography and roughness of biomaterials (Calabrese et al., 2021; Kubo et al., 2009). Furthermore, BNC has gained attention as a vehicle/scaffold for such inorganic particles in tissue engineering field. Its high mechanical strength, large surface area, and capacity for surface modifications make BNC an ideal candidate for development robust and biocompatible scaffolds (He et al., 2021). By combining BNC with inorganic components, novel researchers aim to develop advanced biomaterials that can support ECM synthesis and promote the structural and biochemical signals needed for effective skin and bone tissue regeneration.

In this study, we investigated the expression of three key biomarkers involved in cellular events related to tissue regeneration. We found that BNC-PO₄ significantly influenced F-actin expression in both fibroblast and osteoblast cells. Although type I collagen and fibronectin expression were also observed, no group showed increased expression compared to the control.

4.6.4. Clinical implications of the biological assays

The findings of this study suggest that phosphorylated BNC combined with TiO₂ nanoparticles could offer significant clinical benefits for advanced wound healing and tissue regeneration. The materials demonstrated enhanced cell migration, adhesion, and proliferation in both fibroblasts and osteoblasts, indicating their potential for promoting dermal and bone tissue regeneration. These properties are particularly relevant for treating chronic wounds, such as diabetic ulcers, and post-surgical wounds.

In vitro cytotoxicity testing revealed no significant toxicity, supporting the safety of these materials for clinical use. However, given the oxidative stress potential of TiO₂ nanoparticles, further *in vivo* studies are needed to assess their long-term safety and performance in animal models.

Additionally, the antimicrobial and anti-inflammatory properties of TiO₂ functionalized BNC films further support their potential as advanced wound dressings. These multifunctional materials could provide effective, safe, and accelerated wound healing, addressing both

tissue regeneration and infection control in clinical settings. Further research will be critical to confirm these promising results *in vivo*.

5. Conclusion

Dry bacterial nanocellulose is a versatile material. Depending on storage conditions it retains most of its original surface morphology, although prolonged storage under acidic conditions does lead to some hydrolysis of the surface regions and thus exposing crystalline domains. Phosphorylation of the surface occurs readily with simple reagents allowing for cost effective surface modification, though bacterial nanocellulose appears to lose some of its mechanical properties becoming more brittle in the process. The overall surface morphology of phosphorylated bacterial nanocellulose strongly depends on the storage conditions, ranging from globular surface structures patterned in the overall shape of the starting fibres when stored under basic conditions to ribbon-like cellulose fibres when stored under acidic or neutral conditions for a prolonged period of time. Thus combined phosphorylation, hydration and pH-treatment of surface-dense bacterial nanocellulose may serve as a way to alter the surface of dry bacterial nanocellulose for subsequent use. The introduction of phosphate onto the fibre surface allows for the introduction of nanosized titania with both lactate covered titania and triethanolamine terminated colloidal titania being successfully introduced. Titania in this system has been utilized to adsorb and desorb the broad-spectrum antibiotic tetracycline, with desorption taking place in a delayed manner over the course of several hours to several days. Providing a way to functionally introduce antibiotics onto commercial dry bacteria cellulose sheets. Biological assays indicated that phosphorylation and introduction of nano-sized TiO₂ via TiBALDH or TATT has promising prospects in tissue engineering via improved cell adhesion and wound closure, confirming our initial hypothesis. The steps in the proposed process in creation of functional composite are highly reproducible permitting successful up-scaling. This study provides a foundation for the future development of a broad range of BNC nanocomposites for therapeutic applications specifically in wound healing and tissue regeneration.

Hypothesis statement

Phosphorylation of bacterial nanocellulose dressing material improves its performance in wound closure due to strong interaction of epithelium cells to phosphate functions. It offers an opportunity to incorporate biocompatible mineral particles binding both phosphate ligands and pharmaceuticals, which permits slow release of the latter.

CRedit authorship contribution statement

Troy C. Breijaert: Writing – review & editing, Writing – original draft, Visualization, Investigation, Data curation. **Marina Fontes:** Writing – review & editing, Validation, Investigation, Formal analysis. **Paula de Abreu Fernandes:** Investigation, Formal analysis. **Hernane da Silva Barud:** Writing – review & editing, Supervision, Resources, Investigation. **Sidney J.L. Ribeiro:** Writing – review & editing, Supervision, Funding acquisition. **Gulaim A. Seisenbaeva:** Writing – review & editing, Supervision, Resources, Project administration, Investigation, Funding acquisition, Conceptualization.

Declaration of competing interest

The authors declare that they have no known competing financial interests or personal relationships that could have appeared to influence the work reported in this paper.

Acknowledgements

The authors would like to acknowledge the Swedish Foundation for

International Cooperation in Research and Higher Education (STINT) for financial support of the project BR2019–8506. Dr. H.S: Barud thanks São Paulo Research Foundation (grant number: 2023/17580–1); (CEMASU, FAPESP), Funding process: 2021/11965–3 and Funding Process: 2017/50334–3; National Council of Scientific and Technological Development/CNPq (Grant: 309614/2021–0), National Institutes of Science and Technology (INCTs), INCT Polysaccharides (Grant: 406973/2022–9), INCT Circularity in Polymer Materials (grant no 406925/2022–4), INCT-INFO (National Institute of Photonics). This study was financed by the Coordination of Superior Level Staff Improvement-Brazil(CAPES) - Finance Code 001. Dr. Marina Fontes thanks São Paulo Research Foundation (FAPESP, grant number: 2023/10811–8).

Supplementary materials

Supplementary material associated with this article can be found, in the online version, at [doi:10.1016/j.carpta.2025.100756](https://doi.org/10.1016/j.carpta.2025.100756).

Data availability

Data will be made available on request.

References

- Ait Benhamou, A., Kassab, Z., Nadifyine, M., Salim, M. H., Sehaqui, H., Moubarik, A., et al. (2021). Extraction, characterization and chemical functionalization of phosphorylated cellulose derivatives from giant reed plant. *Cellulose*, 28, 4625–4642. <https://doi.org/10.1007/s10570-021-03842-6>
- Ayorinde, T., & Sayes, C. M. (2023). An updated review of industrially relevant titanium dioxide and its environmental health effects. *Journal of Hazardous Materials Letters*, 4, Article 100085. <https://www.sciencedirect.com/science/article/pii/S2666911023000114>.
- Barud, H. S., Regiani, T., Marques, R. F. C., Lustru, W. R., Messaddeq, Y., & Ribeiro, S. J. L. (2011). Antimicrobial bacterial cellulose-silver nanoparticles composite membranes. *Journal of Nanomaterials*, 2011, 1–8. <https://doi.org/10.1155/2011/721631>
- Breijaert, T. C., Daniel, G., Hedlund, D., Svedlindh, P., Kessler, V. G., Granberg, H., et al. (2022). Self-assembly of ferric – nanocellulose composite fibres. *Carbohydrate Polymers*, 291, Article 119560. <https://doi.org/10.1016/j.carbpol.2022.119560>.
- Brown, A. J. (1886). XIX—The chemical action of pure cultivations of bacterium acetii. *Journal of the Chemical Society, Transactions*, 49, 172–187. <https://doi.org/10.1039/CT8864900172>
- Calabrese, G., Franco, D., Petralia, S., Monforte, F., Condorelli, G. G., Squarzone, S., et al. (2021). Dual-functional nano-functionalized titanium scaffolds to inhibit bacterial growth and enhance osteointegration. *Nanomaterials*, 1, 2634. <https://doi.org/10.3390/nano11102634>
- GVAI-89-97- Capiello, F., Casciaro, B., Mangoni, M.L. (2018). A novel in vitro wound healing assay to evaluate cell migration. *JoVE*, 17:56825. <https://doi.org/10.3791/56825>.
- Choi, S. M., Rao, K. M., Zo, S. M., Shin, E. J., & Han, S. S. (2022). Bacterial cellulose and its applications. *Polymers*, 14(6), 1080. <https://doi.org/10.3390/polym14061080>
- Datta, D., Prajapati, B., Jethva, H., Agrawal, K., Singh, S., & Prajapati, B. G. (2024). Value-added nanocellulose valorized from fruit peel waste for potential dermal wound healing and tissue regenerative applications. *Regenerative Engineering and Translational Medicine*. <https://doi.org/10.1007/s40883-024-00348-y> (in press).
- Ekstrand-Hammarström, B., Hong, J., Davoodpour, P., Sandholm, K., Ekdahl, K. N., Bucht, A., et al. (2015). TiO₂ nanoparticles tested in a novel screening whole human blood model of toxicity trigger adverse activation of the kallikrein system at low concentrations. *Biomaterials*, 51, 58–68. <https://doi.org/10.1016/j.biomaterials.2015.01.031>
- Fink, H.-P., Purz, H. J., Bohn, A., & Kunze, J. (1997). Investigation of the supramolecular structure of never dried bacterial cellulose. In *Macromolecular Symposia*, 120 pp. 207–217. <https://doi.org/10.1002/masy.19971200121>
- French, A. D. (2014). Idealized powder diffraction patterns for cellulose polymorphs. *Cellulose*, 21, 885–896. <https://doi.org/10.1007/s10570-013-0030-4>
- Gaio, S., Svensson, F. G., Breijaert, T. C., Seisenbaeva, G. A., & Kessler, V. G. (2022). Nanoceria–nanocellulose hybrid materials for delayed release of antibiotic and anti-inflammatory medicines. *Materials Advances*, 3, 7228–7234. <https://doi.org/10.1039/D2MA00471B>
- Galkina, O. L., Ivanov, V. K., Agafonov, A. V., Seisenbaeva, G. A., & Kessler, V. G. (2015a). Cellulose nanofiber–titania nanocomposites as potential drug delivery systems for dermal applications. *Journal of Materials Chemistry B*, 3, 1688–1698. <https://doi.org/10.1039/C4TB01823K>
- Galkina, O. L., Öneby, K., Huang, P., Ivanov, V. K., Agafonov, A. V., Seisenbaeva, G. A., et al. (2015b). Antibacterial and photochemical properties of cellulose nanofiber–titania nanocomposites loaded with two different types of antibiotic medicines. *Journal of Materials Chemistry B*, 3, 7125–7134. <https://doi.org/10.1039/C5TB01382H>
- Gan, P., G, Sam, S. T., Abdullah, M. F., bin, & Omar, M. F. (2020). Thermal properties of nanocellulose-reinforced composites: A review. *Journal of Applied Polymer Science*, 137, 48544. <https://doi.org/10.1002/app.48544>
- Gardel, M. L., Schneider, I. C., Aratyn-Schaus, Y., & Waterman, C. M. (2010). Mechanical integration of actin and adhesion dynamics in cell migration. *Annual Review of Cell and Developmental Biology*, 26, 315–333. <https://doi.org/10.1146/annurev.cellbio.011209.122036>
- Groenke, N., Seisenbaeva, G. A., Kaminsky, V., Zhivotovskiy, B., Kost, B., & Kessler, V. G. (2012). Structural characterization, solution stability, and potential health and environmental effects of the Nano-TiO₂ bioencapsulation matrix and the model product of its biodegradation TiBALDH. *RSC Advances*, 2, 4228–4235. <https://doi.org/10.1039/C2RA20388J>
- He, W., Wu, J., Xu, J., Mosselhy, D. A., Zheng, Y., & Yang, S. (2021). Bacterial cellulose functionalization and wound healing applications. *Advances in Wound Care*, 10, 623–640. <https://doi.org/10.1089/wound.2020.1219>
- Horue, M., Silva, J. M., Berti, I. R., Brandão, L. R., Barud, H. D. S., & Castro, G. R. (2023). Bacterial cellulose-based materials as dressings for wound healing. *Pharmaceutics*, 15, 424. <https://doi.org/10.3390/pharmaceutics15020424>
- Inagaki, N., Nakamura, S., Asai, H., & Katsuura, K. (1976). Phosphorylation of cellulose with phosphorous acid and thermal degradation of the product. *Journal of Applied Polymer Science*, 20, 2829–2836. <https://doi.org/10.1002/app.1976.070201017>
- Kanta, J. (2015). Collagen matrix as a tool in studying fibroblastic cell behavior. *Cell Adhesion & Migration*, 9, 308–316. <https://doi.org/10.1080/19336918.2015.1005469>
- Kessler, V. G., Seisenbaeva, G. A., Håkansson, S., & Unell, M. (2008). Chemically triggered biodelivery using metal–organic sol–gel synthesis. *Angewandte Chemie International Edition*, 47, 8506–8509. <https://onlinelibrary.wiley.com/doi/abs/10.1002/anie.200803307>.
- Kessler, V. G., Spijksma, G. I., Seisenbaeva, G. A., Hakansson, S., Blank, D. H., & Bouwmeester, H. J. (2006). New insight in the role of modifying ligands in the sol-gel processing of metal alkoxide precursors: a possibility to approach new classes of materials. *Journal of Sol-Gel Science and Technology*, 40, 163–179.
- Khalid, A., Ullah, H., Ul-Islam, M., Khan, R., Khan, S., Ahmad, F., et al. (2017). Bacterial cellulose–TiO₂ nanocomposites promote healing and tissue regeneration in burn mice model. *RSC Advances*, 7, 47662–47668. <https://doi.org/10.1039/C7RA06699F>
- Khan, S., Ul-Islam, M., Khattak, W. A., Ullah, M. W., & Park, J. K. (2015). Bacterial cellulose–titanium dioxide nanocomposites: nanostructural characteristics, antibacterial mechanism, and biocompatibility. *Cellulose*, 22, 565–579. <https://doi.org/10.1007/s10570-014-0528-4>
- Klemm, D., Heublein, B., Fink, H.-P., & Bohn, A. (2005). Cellulose: fascinating biopolymer and sustainable raw material. *Angewandte Chemie International Edition*, 44, 3358–3393. <https://doi.org/10.1002/anie.200460587>
- Klemm, D., Schumann, D., Urdardt, U., & Marsch, S. (2001). Bacterial synthesized cellulose — Artificial blood vessels for microsurgery. *Progress in Polymer Science*, 26, 1561–1603. [https://doi.org/10.1016/S0079-6700\(01\)00021-1](https://doi.org/10.1016/S0079-6700(01)00021-1)
- Kubo, K., Tsukimura, N., Iwasa, F., Ueno, T., Saruwatari, L., Aita, H., et al. (2009). Cellular behavior on TiO₂ nanonodular structures in the micro-to-nanoscale hierarchy model. *Biomaterials*, 30, 5319–5329. <https://doi.org/10.1016/j.biomaterials.2009.06.021>
- Larsson, D. G. J., & Flach, C. F. (2022). Antibiotic resistance in the environment. *Nature Reviews Microbiology*, 20, 257–269. <https://www.nature.com/articles/s41579-021-00649-x>.
- Le Clairche, C., & Carlier, M.-F. (2008). Regulation of actin assembly associated with protrusion and adhesion in cell migration. *Physiological Reviews*, 88, 489–513. <https://doi.org/10.1152/physrev.00021.2007>
- Li, M., Liang, Y., He, J., Zhang, H., & Guo, B. (2020). Two-pronged strategy of biomechanically active and biochemically multifunctional hydrogel wound dressing to accelerate wound closure and wound healing. *Chemistry of Materials*, 32, 9937–9953. <https://doi.org/10.1021/acs.chemmater.0c02823>
- Li, Y., Jiang, H., Zheng, W., Gong, N., Chen, L., Jiang, X., et al. (2015). Bacterial cellulose–hyaluronan nanocomposite biomaterials as wound dressings for severe skin injury repair. *Journal of Materials Chemistry B*, 3, 3498–3507. <https://doi.org/10.1039/C4TB01819B>
- Li, Y., Tian, Y., Zheng, W., Feng, Y., Huang, R., Shao, J., et al. (2017). Composites of bacterial cellulose and small molecule-decorated gold nanoparticles for treating gram-negative bacteria-infected wounds. *Small*, 13, Article 1700130. <https://doi.org/10.1002/sml.201700130>
- Liao, C., Li, Y., & Tjong, S. C. (2019). Bactericidal and cytotoxic properties of silver nanoparticles. *International Journal of Molecular Sciences*, 20, 449. <https://doi.org/10.3390/ijms20020449>
- Machado, R. T. A., Gutierrez, J., Tercjak, A., Trovatti, E., Uahib, F. G. M., de, P., et al. (2016). Komagataibacter rhaeticus as an alternative bacteria for cellulose production. *Carbohydrate Polymers*, 152, 841–849. <https://doi.org/10.1016/j.carbpol.2016.06.049>
- Malnes, D., Ahrens, L., Köhler, S., Forsberg, M., & Golovko, O. (2022). Occurrence and mass flows of contaminants of emerging concern (CECs) in Sweden's three largest lakes and associated rivers. *Chemosphere*, 294, Article 133825. <https://doi.org/10.1016/j.chemosphere.2022.133825>
- Marchessault, R. H., & Sundararajan, P. R. (1983). Cellulose. *The polysaccharides* (pp. 11–95). Elsevier. <https://doi.org/10.1016/B978-0-12-065602-8.50007-8>
- Morais, D. C., Fontes, M. L., Oliveira, A. B., Gabbai-Arnelin, P. R., Ferrisse, T. M., De Oliveira, F. F. C., et al. (2023). Combining polymer and cyclodextrin strategy for drug release of sulfadiazine from electrospun fibers. *Pharmaceutics*, 15, 1890. <https://doi.org/10.3390/pharmaceutics15071890>

- Moritz, S., Wiegand, C., Wesarg, F., Hessler, N., Müller, F. A., Kralisch, D., et al. (2014). Active wound dressings based on bacterial nanocellulose as drug delivery system for octenidine. *International Journal of Pharmaceutics*, *471*, 45–55. <https://doi.org/10.1016/j.ijpharm.2014.04.062>
- Myers, H. M., Tochon-Danguy, H. J., & Baud, C. A. (1983). IR absorption spectrophotometric analysis of the complex formed by tetracycline and synthetic hydroxyapatite. *Calcified Tissue International*, *35*, 745–749. <https://doi.org/10.1007/BF02405117>
- O'Sullivan, A. C. (1997). Cellulose: the structure slowly unravels. *Cellulose*, *4*, 173–207. <https://doi.org/10.1023/A:1018431705579>
- Paladini, F., & Pollini, M. (2019). Antimicrobial silver nanoparticles for wound healing application: progress and future trends. *Materials (Basel)*, *12*, 2540. <https://doi.org/10.3390/ma12162540>
- Parisi, L., Toffoli, A., Ghezzi, B., Mozzoni, B., Lumetti, S., & Macaluso, G. M. (2020). A glance on the role of fibronectin in controlling cell response at biomaterial interface. *Japanese Dental Science Review*, *56*, 50–55. <https://doi.org/10.1016/j.jdsr.2019.11.002>
- Paschoalin, R. T., Traldi, B., Aydin, G., Oliveira, J. E., Rütten, S., Mattoso, L. H. C., et al. (2017). Solution blow spinning fibres: new immunologically inert substrates for the analysis of cell adhesion and motility. *Acta Biomaterialia*, *51*, 161–174. <https://doi.org/10.1016/j.actbio.2017.01.020>
- Patoary, M. K., Farooq, A., Zaarour, B., & Liu, L. (2021). Phosphorylated cellulose nanofibrils: structure-morphology-rheology relationships. *Cellulose*, *28*, 4105–4117. <https://doi.org/10.1007/s10570-021-03786-x>
- Rasouli, M., Soleimani, M., Hosseinzadeh, S., & Ranjbari, J. (2023). Bacterial cellulose as potential dressing and scaffold material: toward improving the antibacterial and cell adhesion properties. *Journal of Polymers and the Environment*, *31*, 4621–4640. <https://doi.org/10.1007/s10924-023-02779-0>
- Rueden, C. T., Schindelin, J., Hiner, M. C., DeZonia, B. E., Walter, A. E., Arena, E. T., et al. (2017). ImageJ2: ImageJ for the next generation of scientific image data. *BMC Bioinformatics*, *18*, 529. <https://doi.org/10.1186/s12859-017-1934-z>
- Seisenbaeva, G. A., Daniel, G., Nedelec, J. M., & Kessler, V. G. (2013). Solution equilibrium behind the room-temperature synthesis of nanocrystalline titanium dioxide. *Nanoscale*, *5*, 3330–3336. <https://pubs.rsc.org/en/content/articlelanding/2013/nr/c3nr34068f>
- Seisenbaeva, G. A., Fromell, K., Vinogradov, V. V., Terekhov, A. N., Pakhomov, A. V., Nilsson, B., et al. (2017). Dispersion of TiO₂ nanoparticles improves burn wound healing and tissue regeneration through specific interaction with blood serum proteins. *Scientific Reports*, *7*, 15448. <https://doi.org/10.1038/s41598-017-15792-w>
- Skocaj, M., Filipic, M., Petkovic, J., & Novak, S. (2011). Titanium dioxide in our everyday life; is it safe? *Radiology and Oncology*, *45*(4), 227–247. <https://pubmed.ncbi.nlm.nih.gov/22933961/>
- Stoica, A. E., Chircov, C., & Grumezescu, A. M. (2020). Nanomaterials for wound dressings: an up-to-date overview. *Molecules*, *25*, 2699. <https://doi.org/10.3390/molecules25112699>
- Suneetha, M., Kim, H., & Han, S. S. (2024). Bone-like apatite formation in biocompatible phosphate-crosslinked bacterial cellulose-based hydrogels for bone tissue engineering applications. *International Journal of Biological Macromolecules*, *256*, Article 128364. <https://doi.org/10.1016/j.ijbiomac.2023.128364>
- Svensson, F. G., Manivel, V. A., Seisenbaeva, G. A., Kessler, V. G., Nilsson, B., Ekdahl, K. N., et al. (2021). Hemocompatibility of nanotitania-nanocellulose hybrid materials. *Nanomaterials*, *11*, 1100. <https://doi.org/10.3390/nano11051100>
- Thomas, L. C., & Chittenden, R. A. (1964b). Characteristic infrared absorption frequencies of organophosphorus compounds—I The phosphoryl (P=O) group. *Spectrochimica Acta*, *20*, 467–487. [https://doi.org/10.1016/0371-1951\(64\)80043-6](https://doi.org/10.1016/0371-1951(64)80043-6)
- Thomas, L. C., & Chittenden, R. A. (1964a). Characteristic infrared absorption frequencies of organophosphorus compounds—II. P-O(X) bonds. *Spectrochimica Acta*, *20*, 489–502. [https://doi.org/10.1016/0371-1951\(64\)80044-8](https://doi.org/10.1016/0371-1951(64)80044-8)
- Theorens, G., Krier, F., Leclercq, B., Carlin, B., & Evrard, B. (2014). Microcrystalline cellulose, a direct compression binder in a quality by design environment—A review. *International Journal of Pharmaceutics*, *473*, 64–72. <https://doi.org/10.1016/j.ijpharm.2014.06.055>
- Tripathi, N., & Goshisht, M. K. (2022). Recent advances and mechanistic insights into antibacterial activity, antibiofilm activity, and cytotoxicity of silver nanoparticles. *ACS Applied Bio Materials*, *5*, 1391–1463. <https://doi.org/10.1021/acsbam.2c00014>
- Volova, T. G., Shumilova, A. A., Shidlovskiy, I. P., Nikolaeva, E. D., Sukovaty, A. G., Vasiliev, A. D., et al. (2018). Antibacterial properties of films of cellulose composites with silver nanoparticles and antibiotics. *Polymer Testing*, *65*, 54–68. <https://doi.org/10.1016/j.polymertesting.2017.10.023>
- Wada, M., Okano, T., & Sugiyama, J. (2001). Allomorphs of native crystalline cellulose I evaluated by two equatorial spacings. *Journal of Wood Science*, *47*, 124–128. <https://doi.org/10.1007/BF00780560>
- Wahid, F., Zhao, X.-J., Zhao, X.-Q., Ma, X.-F., Xue, N., Liu, X.-Z., et al. (2021). Fabrication of bacterial cellulose-based dressings for promoting infected wound healing. *ACS Applied Materials & Interfaces*, *13*, 32716–32728. <https://doi.org/10.1021/acsmi.1c06986>
- Zahel, P., Beekmann, U., Eberlein, T., Schmitz, M., Werz, O., & Kralisch, D. (2022). Bacterial cellulose—adaptation of a nature-identical material to the needs of advanced chronic wound care. *Pharmaceuticals (Basel)*, *15*(6), 683. <https://doi.org/10.3390/ph15060683>
- Zhangjian Chen, Z., Han, S., Zhou, S., Feng, H., Liu, Y., & Jia, G. (2020). Review of health safety aspects of titanium dioxide nanoparticles in food application. *Nano Impact*, *18*, Article 100224. <https://www.sciencedirect.com/science/article/pii/S2452074820300185>